

Comparative Electromagnetic Performance of Axial Flux Permanent Magnet Motors with Three Different Rotor Topologies

Xuyang Liu¹, Xue Yu¹, Junjie Jiang¹, Yu Wang²

¹ Nanjing University of Science and Technology, Nanjing 210094, China

² Fudan University, Shanghai 200433, China

(Corresponding Author: Weiwei Geng Email: gww@njust.edu.cn)

ABSTRACT

Dual-stator axial flux permanent magnet motors (DSSR-AFPM) have been widely applied in electric vehicle drive systems due to their high torque density and compact structure. However, most existing DSSR-AFPM motors employ a surface-mounted permanent magnet (SPM) rotor topology, which suffers from the inability to utilize reluctance torque, high harmonic content in the air-gap flux density, and significant torque ripple. To overcome these drawbacks, this paper proposes a novel interior permanent magnet (NIPM) rotor with magnetic isolation slots. Under identical design constraints, the electromagnetic performances of three rotor topologies—SPM, surface-embedded permanent magnet (SEPM), and NIPM—are compared using three-dimensional finite element analysis. The results show that the NIPM rotor achieves a more sinusoidal air-gap flux distribution, reduced torque ripple, and enhanced flux-weakening capability, while maintaining high efficiency over a wide speed range.

Keywords: Axial-flux permanent magnet machine, Dual-stator single rotor, Torque/power density, flux-weakening speed expansion

1. INTRODUCTION

Growing environmental pollution and the drive to achieve carbon neutrality have positioned electric vehicles as a key transportation solution. Consequently, the drive motor—their primary power source—is gaining significant attention from researchers and industry experts. Permanent magnet synchronous motor (PMSM) are the primary choice for electric vehicle drives due to their high power density, efficiency, and brushless design. Based on flux path, PMSM are categorized as axial flux or radial flux types. Study [1] compared the performance and size of RFPM motors against four AFPM motors configurations (single-stator single-rotor,

double-stator single-rotor, and their slotless variants) across five power levels. Their analysis demonstrated that AFPM motors are generally more compact at equivalent power. Specifically, AFPM motors designs exhibit lower rotational inertia and reduced effective weight when using identical permanent magnet materials and air gap flux density.

Consequently, AFPM motors enhance electric vehicle power capacity and facilitate chassis layout optimization. As EVs advance towards higher performance and longer range, their drive motors require greater power density and improved thermal management. Meeting standards like FreedomCAR 2020—which mandates peak speeds of at least 14000 r/min—further underscores these demands [2]. The pursuit of high-speed drive motors presents significant challenges for AFPM motors.

Current AFPM motors research predominantly focuses on rotor optimization through permanent magnet (PM) installation methods, PM shaping, and flux barrier design. Most dual-stator single-rotor AFPM motors (DSSR-AFPM) employ surface-mounted permanent magnet (SPM) rotors. This configuration relies solely on PM torque, limiting total output and exhibiting poor constant-power operation. With rising PM costs prioritizing motor economics, power per unit magnet volume becomes critical. Built-in permanent magnet (IPM) designs address this via integrated flux barriers that create d/q-axis inductance saliency, generating supplemental reluctance torque. Crucially, SPM motors require higher d-axis flux-weakening currents than IPM equivalents to achieve comparable field-weakening capability. This necessitates larger drive capacity; moreover, excessive d-axis demagnetizing current increases losses, reduces efficiency, and risks irreversible PM demagnetization.

This paper therefore proposes an IPM rotor structure with three parallel PM rows and end-mounted flux

barriers to suppress leakage flux. Using finite element analysis, we compare electromagnetic performance—including air-gap flux density, field distribution, torque output, torque density, and power density—across three rotor topologies. Subsequent loss quantification and efficiency analysis provide a validated topology reference for DSSR-AFPM motor design.

2. DIFFERENT ROTOR TOPOLOGIES OF DSSR-AFPM MOTORS

SPMs dominate as the preferred rotor topology owing to their straightforward installation. However, the SPM design exhibits equal d-axis and q-axis inductances, eliminating reluctance torque. This results in limited performance within the constant power operating region. In contrast, the IPM configuration utilizes flux barriers to generate significant reluctance torque. When achieving equivalent flux weakening, the SPM design requires a larger direct-axis demagnetizing current than the IPM design. Consequently, it necessitates increased drive capacity. Furthermore, excessive demagnetizing current raises motor losses, reduces efficiency, and poses risks of irreversible permanent magnet demagnetization. This paper proposes a built-in parallel three-row PM rotor topology. Magnetic isolation slots incorporated on either side of the PMs guide rotor core flux, minimizing leakage flux.

This study compares the effects of three rotor topologies on motor performance: Surface-Mounted Permanent Magnet (SPM), Surface-Embedded Permanent Magnet (SEPM), and New Interior Permanent Magnet (NIPM). This comparison provides design guidance for selecting rotor configurations in subsequent DSSR-AFPM development.

TABLE I
PARAMETERS OF THE THREE MOTORS

Parameters	SPM	SEPM	NIPM
Number of Poles/Slots	12/72		
Stator/Rotor Inner/Outer Diameter/mm	160/250		
Airgap Length(Single-side)/mm	1.3		
Slot-filling Factor	0.42		
PM Material	G52UH		
Core Material	25SW1300		
Axial Length/mm	61.6	61.6	68.6
PM Mass/kg	1.08	1.08	1.08

To ensure a valid comparison, the following design constraints are applied:

1) All configurations maintain identical stator inner/outer diameters and pole-slot combinations. The effective axial length is optimized in consideration of the

electromagnetic performances, and is not exceed 70 mm.

2) All the motors use N52UH as PM material and the amounts of N52UH are consist. Both stators and rotors use the same grade of silicon steel (trademark 25SW1300 in China).

3) All configurations maintain identical permanent magnet quantities.

4) All configurations employ identical oil-cooled thermal management systems, ensuring consistent current density and standardized windings.

The three topologies are illustrated in Fig. 1. The specific parameters are shown in Table I.

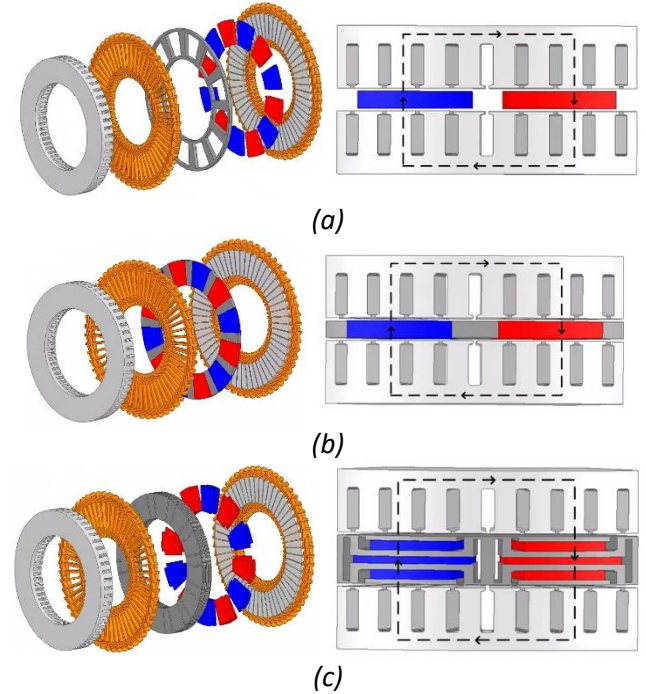


Fig. 1 (a) Surface-mounted permanent magnet (SPM) rotor topology. (b) Surface-mounted embedded permanent magnet (SEPM) rotor topology. (c) New interior permanent magnet (NIPM) rotor topology.

3. ELECTROMAGNETIC PERFORMANCE ANALYSIS

This section models the motor under the specified constraints and compares fundamental electromagnetic performance of the three rotor topologies using finite element analysis. The analysis assesses no-load operation, on-load characteristics, and loss distributions. Comparative metrics include mass, torque density, power density, and peak efficiency.

3.1 Open-Circuit

Fig. 2 presents the magnetic circuits and flux density distributions of all three topologies under no-load conditions. To ensure equitable comparison, the saturation of the three motors is relatively similar. The

main parts of saturation are concentrated in the rotor yoke and stator teeth.

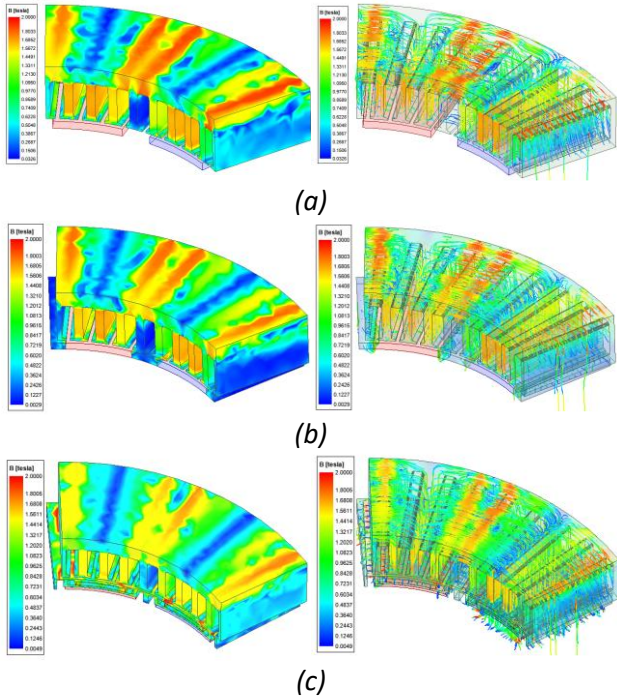


Fig. 2 Field distributions and flux density under no-load. (a)SPM. (b)SEPM. (c)NIPM.

Fig. 3 compares no-load air-gap flux density and its FFT spectrum across the three topologies. SPM and SEPM exhibit similar flux density amplitudes, fundamental amplitudes are 0.97 T and 0.94 T, respectively. The NIPM shows a 12.4% reduction relative to SPM, despite magnetic isolation slots incorporated alongside the permanent magnets to minimize leakage flux, residual flux leakage persists. This results in reduced air-gap flux density amplitude in the NIPM configuration. Notably, NIPM's unique magnet arrangement configuration yields a more sinusoidal air-gap flux density waveform with significantly lower harmonic content. This results in substantially reduced cogging torque and torque ripple compared to conventional topologies.

The reduced air-gap flux density amplitude decreases the no-load back EMF amplitude as shown in Fig. 4. FFT further confirms significantly lower higher-order harmonics in the NIPM topology compared to both SPM and SEPM configurations.

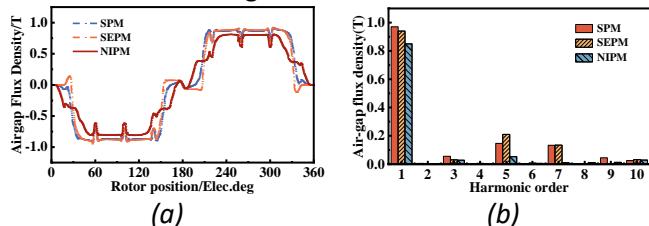


Fig. 3 Airgap flux density. (a)Airgap flux density. (b)FFT.

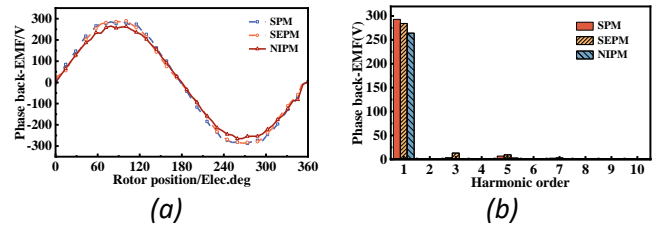


Fig. 4 Back EMF. (a)Back EMF. (b)FFT.

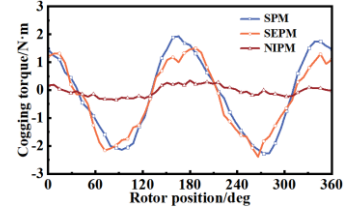


Fig. 5 Cogging torque of three comparative motors.

3.2 On-Load

Three-dimensional finite element analysis (3D-FEA) characterizes output torque versus current relationships across rotor topologies. To ensure equitable comparison, SEPM and NIPM topologies employ Maximum Torque Per Ampere (MTPA) control. Fig. 6 demonstrates optimized reluctance torque utilization through current angle sweeps, maximizing output torque at given current levels. It can be seen from the average torque verses to phase current curve, as shown in Fig. 7, when the key factors such as the mass of the permanent magnet, the inner diameter and the outer diameter of the motor are constant, the output torque capability of the SPM is slightly higher than that of other motors. However, under heavy load conditions, the output torque capacity of NIPM is larger, and the advantage of reluctance torque is more obvious. It can be seen from the output torque waveform (Fig. 8) of the same load that the torque ripple of NIPM is much smaller than that of other motors.

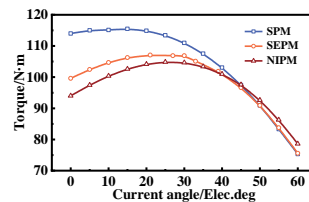


Fig. 6 Average torque verses to phase current angle.

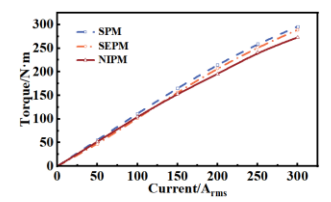


Fig. 7 Average torque verses to phase current.

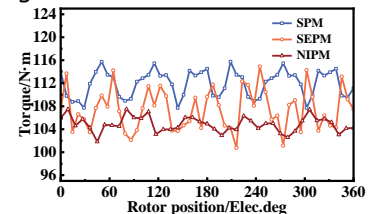


Fig. 8 Output torque waveform under the same load.

The characteristic current is defined as the d-axis current required to drive the d-axis flux linkage to zero

under flux-weakening operation. This parameter serves as a critical metric for evaluating permanent magnet motor flux-weakening capability, quantified by:

$$I_c = \frac{\Psi_{PM}}{L_d} \quad (1)$$

where Ψ_{pm} is the permanent magnet flux linkage, and L_d is the d -axis inductance.

Fig. 9 reveals significantly lower characteristic current for NIPM (259.75 A) versus SPM and SEPM designs. This results from NIPM's reduced d -axis inductance relative to other topologies.

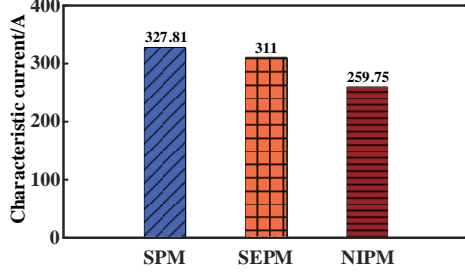


Fig. 9 RMS characteristic current for all three motors.

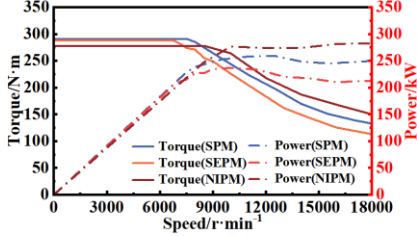


Fig. 10 Torque-speed curves and power-speed curves.

The d/q axis inductance of the three motors is shown in Table II. Compared with other motors, the d/q axis inductance of NIPM has the largest difference and the highest saliency ratio, which effectively improves the reluctance torque output capacity.

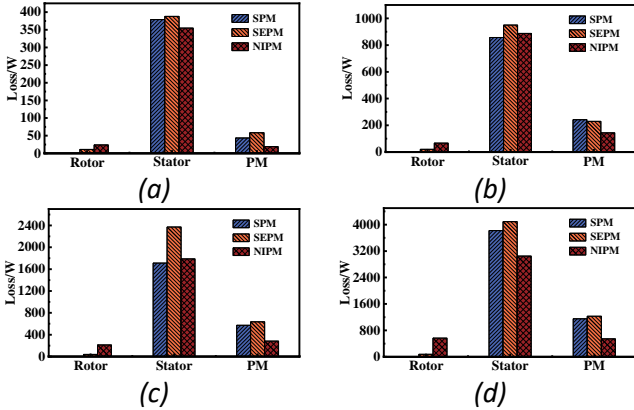


Fig. 11 Loss analysis under typical working conditions. (a) $i_d=0$ A $i_q=150$ A 3000 r/min. (b) $i_d=0$ A $i_q=300$ A 5000 r/min. (c) $i_d=173$ A $i_q=100$ A 10000 r/min. (d) $i_d=153$ A $i_q=128$ A 15000 r/min.

3D-FEA yields the torque-speed characteristics of all three topologies, shown in Fig. 10. Although the peak torque of SPM is slightly higher than that of NIPM, NIPM

exhibits better peak power and flux-weakening capability. The peak power can reach 282 kW, power mass density is 18.59.

TABLE II
INDUCTANCE COMPARISON OF THREE MOTORS

Machine type	$L_d/\mu H$	$L_q/\mu H$
SPM	284	279
SEPM	290	510
NIPM	323	608

3.3 Loss And Efficiency

Fig. 11 compares loss distributions across three topologies at four operating points. SPM exhibits zero rotor core loss due to its non-laminated rotor structure. From the results in the diagram, it can be seen that the stator core loss and permanent magnet eddy current loss of SEPM are larger than those of the other two motors at both low and high speeds. Because the rotor core of NIPM is larger than that of other motors, the rotor core loss is larger, and the stator core loss and permanent magnet eddy current loss are smaller.

Fig. 12 presents efficiency maps for all three topologies, revealing broadly similar high-efficiency regions. Peak efficiencies reach 95.4% (SPM), 95.3% (SEPM), and 95.8% (NIPM). Table III quantifies and compares torque density and power density across all three topologies.

TABLE III
COMPARISON OF TORQUE DENSITY AND POWER DENSITY

Parameters	SPM	SEPM	NIPM
Peak power/kW	249	236	282
Peak torque/N·m	295	288	273
Effective material weight/kg	13.74	14.21	15.17
Power mass density/kW/kg	18.1	16.6	18.59
Torque mass density/N·m/kg	21.47	20.26	18
Highest efficiency	95.4%	95.3%	95.8%

4. CONCLUSIONS

This paper comparatively analyzes three rotor topologies for DSSR-AFPMSM. Under fixed permanent magnet constraints, finite element analysis evaluates torque characteristics, power density, loss distribution, flux-weakening capability, and efficiency. Key findings are summarized as follows:

(1) The results show that the output torque capability of SPM is slightly higher than that of SEPM and NIPM under the same amount of permanent magnet. Although NIPM sets magnetic isolation slots on both sides of the permanent magnet to prevent magnetic

leakage between poles, a small amount of magnetic leakage is inevitable, resulting in a decrease in air gap flux density and a limited torque output capacity. It is necessary to optimize the design of the magnetic isolation slot to reduce the inter-pole magnetic flux leakage and improve the torque output capability. Compared with the other two motors, NIPM has higher peak power and stronger flux-weakening ability. It is suitable for applications with high speed and high load.

(2) The permanent magnet setting method of NIPM can optimize the air gap flux density waveform, make the waveform more sinusoidal, and effectively reduce the harmonic content. The motor has lower cogging torque and torque ripple.

(3) NIPM has a lower characteristic current, indicating that the weak magnetic ability is stronger. The salient pole ratio can reach 2, which can make better use of the reluctance torque to increase the output torque.

(4) NIPM has lower core loss and permanent magnet eddy current loss under high speed and high load conditions, and has higher efficiency. It can show advantages in high-power and high-speed applications.

REFERENCE

[1] Sitapati K, Krishnan R. Performance comparisons of radial and axial field, permanent-magnet, brushless machines[J]. IEEE Transactions on industry applications, 2001.37(5):1219-1226

[2] A.M.EL-Refaie et al., "Advanced high-power-density interior permanent magnet motor for traction applications," IEEE Trans. Ind. Appl., vol. 50, no. 5, pp. 3235-3248, Sep./Oct. 2014, doi: 10.1109/TIA.2014.2305804.

[3] Y. Cheng, L. Ding, T. Zhao and S. Cui, "Design and Optimization of Electric Vehicle Traction Motor Considering Rotor Topology and Manufacturing Uncertainty," in IEEE Transactions on Industrial Electronics, vol. 71, no. 5, pp. 5034-5044, May 2024, doi: 10.1109/TIE.2023.3288195.

[4] G. Dajaku, "Analytical Analysis of Electromagnetic Torque and Magnet Utilization Factor for Two Different PM Machines With SPM and HUPM Rotor Topologies," in IEEE Transactions on Magnetics, vol. 57, no. 6, pp. 1-9, June 2021, Art no. 8106309, doi: 10.1109/TMAG.2021.3069082.

[5] S. Li, W. Tong, S. Wu and R. Tang, "Analytical Model for Electromagnetic Performance Prediction of IPM Motors Considering Different Rotor Topologies," in IEEE Transactions on Industry Applications, vol. 59, no. 4, pp. 4045-4055, July-Aug. 2023, doi: 10.1109/TIA.2023.3268639.

[6] A. Wang, Y. Jia and W. L. Soong, "Comparison of Five Topologies for an Interior Permanent-Magnet Machine for a Hybrid Electric Vehicle," in IEEE Transactions on Magnetics, vol. 47, no. 10, pp. 3606-3609, Oct. 2011, doi: 10.1109/TMAG.2011.2157097.

[7] S. Cai, Z. Q. Zhu, S. Mallampalli, J.C. Mipo and S. Personnaz, "Investigation of Novel Fractional Slot Nonoverlapping Winding Hybrid Excited Machines With Different Rotor Topologies," in IEEE Transactions on Industry Applications, vol. 57, no. 1, pp. 468-480, Jan.-Feb. 2021, doi: 10.1109/TIA.2020.3040347.

[8] W. Cheng, G. Cao, Z. Deng, L. Xiao and M. Li, "Torque Comparison Between Slotless and Slotted Ultra-High-Speed AFPM Motors Using Analytical Method," in IEEE Transactions on Magnetics, vol. 58, no. 2, pp. 1-5, Feb. 2022, Art no. 8101805, doi: 10.1109/TMAG.2021.3081175.

[9] A. W. Bandarkar, M. K. Mahmud Bin Azam and Y. Sozer, "Comparative Performance Analysis of Slotted and Slotless Dual-Stator and Single-Rotor Axial-Flux Permanent Magnet Motor for Integrated Motor-Compressor System," in IEEE Transactions on Industry Applications, vol. 61, no. 3, pp. 4234-4245, May-June 2025, doi: 10.1109/TIA.2025.3541164.

[10] L. Jia, K. Lin, M. Lin, W. Le and S. Wang, "Comparative Analysis of Dual-Rotor Modular Stator Axial-Flux Permanent Magnet Machines With Different Rotor Topologies," in IEEE Transactions on Applied Superconductivity, vol. 31, no. 8, pp. 1-5, Nov. 2021, Art no. 5204405, doi: 10.1109/TASC.2021.3091124.